PAPER

Check for updates

Precursor preparation of Zn–Al layered double hydroxide by ball milling for enhancing adsorption and photocatalytic decoloration of methyl orange

Jun Qu,[*a] Xiaoman He,[a] Xuewei Li,[a] Ziqiang Ai,[a] Yujie Li,[a] Qiwu Zhang [ID] [*a] and Xinzhong Liu[b]

An amorphous photocatalyst was prepared *via* simple dry milling of Zn basic carbonate ($Zn_4CO_3(OH)_6 \cdot H_2O$) and Al hydroxide ($Al(OH)_3$) as a precursor of Zn–Al layered double hydroxide (LDH) and the precursor was agitated in water to simply synthesize the Zn–Al LDH for comparison. The adsorption and photocatalytic activity of the Zn–Al LDH and the precursor were studied *via* the removal of methyl orange (MO) and decoloration of MO under ultraviolet light irradiation in aqueous solution, respectively. The precursor exhibits much higher decoloration efficiency towards MO than the Zn–Al LDH product because of the synergistic effect of the intercalation reaction and its photocatalytic activity. The amorphous precursor could easily incorporate MO molecules to form MO intercalated LDH, allowing easy access of the organic pollutant to the photocatalyst sample, resulting in an obvious improvement in photocatalytic performance. The novel idea to use the precursor sample instead of the synthesized final product may be applied in other fields to increase the required performances.

1 Introduction

Layered double hydroxides (LDH), also known as anion clays or hydrotalcite-like compounds, with zinc or titanium located in their sheets have been widely used as photocatalysts[1] for the degradation of organic pollutants or water-splitting.[2,3] No photocatalytic properties were reported with Mg–Al LDHs, whereas the ternary Mg–Zn–Al LDH formed with zinc was found to be able to degrade organic pollutants under light irradiation,[4] and high photocatalytic performance was obtained when Mg was entirely replaced by Zn, forming the binary Zn–Al LDH. There has been much work on the synthesis and modification of Zn–Al to enhance its photocatalytic activity. Dutta *et al.*[5] synthesized a composite with Zn–Al LDH and ZnO and reported high efficiency for the decomposition of Congo Red. Lin *et al.*[6] proposed a method to manufacture titanate-intercalated Zn–Al LDH and demonstrated its superior photocatalytic activity. Carriazo *et al.*[7] studied the photocatalytic activity of Zn–Al LDH calcined at different temperatures. In these reports, significant attention was paid to control the morphology of LDH or develop composite catalysts with precious metals. These elaborate efforts will surely increase the cost of production and thus limit the actual value of these materials in practical applications.[8,9]

Tongamp *et al.*[10,11] first reported a solvent-free mechanochemical method (two-step milling: dry milling followed by wet milling) to synthesize Mg–Al LDH. Subsequently, other types of LDH were fabricated.[12] Qu *et al.*[13–15] synthesized Ca–Al LDH, Li–Al LDH and tetraborate pillared Li–Al *via* the two-step milling method and Ferencz *et al.*[16,17] prepared Ca–Fe and Ca–Sn LDH in the same manner. The reported mechanochemical approach based on solid state reaction exhibits some obvious advantages such as no need for heating treatment and no discharge of waste water as in the traditional hydrothermal process. Recently improvements in the adsorption of target pollutants were observed with the mechanochemically prepared LDH products. The dry milling sample, which is known as the precursor, was found to be an excellent anion adsorbent toward anion organic or inorganic pollutants in our recently published works. Wang *et al.*[18] compared the MO adsorption performance of the precursor of Mg–Al LDH, which was prepared by the dry milling of magnesium hydroxide and aluminum hydroxide, with that of well-crystallized Mg–Al LDH products and found that the precursor showed an obviously higher adsorption capacity toward MO. The precursor of ettringite, which was prepared by the dry milling of dihydrate calcium sulfate, calcium hydroxide and aluminum hydroxide, also possessed a much higher adsorption capacity toward phosphate than that of ettringite.[19] However, the abovementioned work is limited to the area of anion adsorption. Thus, more work is needed to broaden the application of mechanochemically prepared precursors.

Close contact between the photocatalyst and the organic pollutant is essential for the photocatalytic reaction, which is

[a]*School of Resources and Environmental Engineering, Wuhan University of Technology, Luoshi Road 122, Wuhan, Hubei 430070, China. E-mail: zhangqw@whut.edu.cn; forsjun@whut.edu.cn; Tel: +86 17771490085*

[b]*College of Ecological Environment and Urban Construction, Fujian University of Technology, Fuzhou 350118, China*

believed to have a massive impact on the photocatalytic efficiency. Extensive research has been conducted to enhance the access of photocatalysts to target pollutants, whether by increasing the specific surface area of the photocatalyst or dispersing the photocatalyst in porous supporting materials such as diatomite.[3,20] However, such elaborate efforts usually increase the production cost, therefore it is difficult to use these materials to purify contaminated water.

Our recent work[18] proved that the precursor of Mg–Al LDH prepared by ball-milling exhibits a much higher adsorption capacity than that of the synthesized adsorbent which was mainly realized by surface adsorption. Herein, based on our recently reported phenomenon that the precursor exhibits much higher adsorption capacity than the synthesized adsorbent, we prepare an amorphous photocatalyst (the precursor of Zn–Al LDH) by simply dry-milling $Zn_4CO_3(OH)_6 \cdot H_2O$ and $Al(OH)_3$ to introduce further photocatalytic activity besides the enhanced adsorption performance. The precursor is found to show much better adsorption and photocatalytic performance toward MO than the well-crystallized Zn–Al LDH, which indicates that the precursor may achieve both easy access to the target by adsorption and decoloration by catalysis. It is believed that such easily prepared precursor meets both the requirements of low cost and high performance and would contribute to the purification of waste water. As a reference experiment, the cationic organic molecule rhodamine B (RHB), which cannot be adsorbed by the LDH, is also used to compare the photocatalytic actions between the precursor and Zn–Al LDH samples.

2 Experimental

2.1 Materials and methods

$Zn_4CO_3(OH)_6 \cdot H_2O$ and $Al(OH)_3$ (Sinopharm Group Co Ltd., China, analytical reagent) were used as raw materials with no further purification. A planetary ball mill (Pulverisette-7, Fritsch, Germany), which has two mill pots (45 cm³ inner volume each) made of zirconium dioxide with 7 zirconium dioxide balls of 15 mm in diameter, was used to conduct the ball-milling operation. Methyl orange ($C_{14}H_{14}N_3SO_3Na$, Aladdin®, China, content 96%) and rhodamine B ($C_{28}H_{31}ClN_2O_3$, Aladdin®, China, analytical reagent) were applied to simulate organic contaminated waste water.

A two-step operation was used for the synthesis of the precursor and Zn–Al LDH. In the first dry grinding process, 2 g of basic zinc carbonate and $Al(OH)_3$ (Zn/Al molar ratio of 2/1) mixture was ground on a planetary ball mill for two hours at 600 rpm to obtain the precursor. In the second agitation step, 1 g of the precursor was put into a capped Erlenmeyer flask filled with 100 mL of distilled water and stirred for 4 hours on a magnetic stirring apparatus (524G, Meiyingpu, China) at 1200 rpm to fabricate Zn–Al LDH.

2.2 Characterization

XRD analysis was used to identify the phases and phase changes of the samples on a powder diffractometer (MAX-RB RU-200B, Rigaku, Japan) using CuKα radiation ($\lambda = 1.5403$ Å) in the 2θ

range of 5° and 70°. The microstructures of the prepared samples were observed on a scanning electron microscope (JSM-5610LVJEOL, Jeol, Japan). FT-IR spectra of the samples were obtained on Nicolet 6700, Thermo, America, using KBr as a diluent over 4000–500 cm⁻¹. A UV/VIS/NIR spectrometer (Lambda 750 S, PerkinElmer, America) was used to record the UV-vis diffusive reflectance spectra of the prepared samples.

2.3 Adsorption and photocatalytic activity

2.3.1 Adsorption activity. For the adsorption kinetic experiments 0.8 g of the as-prepared samples was continuously stirred in 1000 mL MO (100 ppm) solution by an electromotive stirrer. 4 mL suspension was collected and centrifuged to remove the adsorbent at given time intervals (0–120 min). The absorbance of the centrifuged solutions at 453 nm for MO was recorded on a UV/VIS spectrometer (UVmini-1240, SHIMADZU, Japan) to calculate the removal efficiency of MO. For the adsorption isotherm experiments 0.08 g of the as-prepared samples was continuously stirred in 100 mL MO solution containing a certain amount of MO (25–350 ppm) on a magnetic stirring apparatus (524G, Meiyingpu, China) at room temperature for 4 hours. Subsequently, the suspensions were centrifuged and 4 mL of the supernatant solutions were taken and analyzed on the UV/VIS spectrometer at 453 nm to calculate the adsorption capacity. For a clear presentation of the text, the LDH sample and the precursor sample with MO adsorption (0.8 g of the sample stirred in 100 mg L⁻¹ MO solution for 120 min) are denoted as L-MO-LDH and P-MO-LDH, respectively.

2.3.2 Photocatalytic activity. The photocatalytic activity of the as-prepared samples was evaluated by the ultraviolet light irradiation of MO and RHB solutions on a photocatalytic reaction instrument (PLS-LAM254, PerfectLight®, China), where the wavelength of the UV light was 254 nm. 0.25 g and 0.2 g of the as-prepared samples were continuously stirred in 250 mL RHB (4 ppm) and MO (100 ppm) solutions with or without light irradiation. 4 mL suspension was collected and centrifuged to remove the photocatalyst at given time intervals. The absorbance of the centrifuged solutions was recorded on a UV/VIS spectrometer (UVmini-1240, SHIMADZU, Japan) at 453 nm for MO and 556 nm for RHB to calculate the decoloration of MO and RHB. Blank experiments without catalyst were also conducted for comparison.

3 Results and discussion

3.1 Results

Our previous study[18] demonstrated the feasibility of manufacturing LDH *via* a mechanochemical route in which $Mg(OH)_2$ and $Al(OH)_3$ are first activated by dry ball milling to obtain the precursor and then stirred in water to prepare Mg–Al LDH. Thus, a similar mechanochemical approach was applied to fabricate Zn–Al LDH and its precursor using $Zn_4CO_3(OH)_6 \cdot H_2O$ and $Al(OH)_3$ as raw materials. Fig. 1 depicts the XRD patterns of the raw materials mixture, the precursor (prepared by dry milling of raw materials at 600 rpm with Zn/Al molar ratio at 2/1) and Zn–Al LDH (fabricated by agitating the precursor in
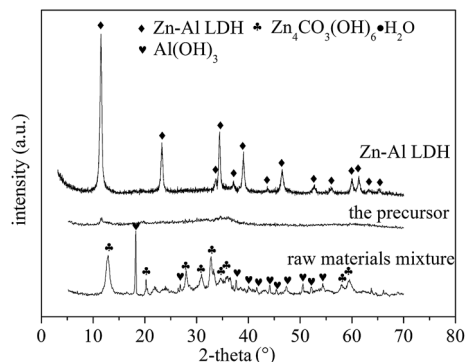
Fig. 1 XRD patterns of the raw materials mixture, precursor (prepared by dry milling of raw materials at 600 rpm) and Zn–Al LDH (fabricated by agitating the precursor in water).

water). The diffraction peaks of $Zn_4CO_3(OH)_6 \cdot H_2O$ and $Al(OH)_3$ were observed in the XRD patterns of the raw materials. After the dry milling operation, an amorphous sample, namely the precursor, was obtained. Agitating the precursor in water at room temperature resulted in the formation of Zn–Al LDH (JCPDS card 48-1022) with the d_{003} value of 0.77 nm.

To show the microstructure of the precursor and LDH, the SEM photographs of the precursor and Zn–Al LDH are displayed in Fig. 2. The particles in the precursor sample formed large thick-massive agglomerates without an evident layered

structure. When the precursor was agitated in water to prepare the LDH sample, a sheet structure was observed. The agitation operation helped the grain growth of crystalline Zn–Al LDH. In this work, we evaluated the adsorption as well as the photocatalytic performance of the Zn–Al LDH precursor toward MO. The Zn–Al LDH prepared by grinding and agitation operation here was also studied under the same conditions for comparison.

The excellent adsorption performances of the Mg–Al LDH precursor[18] and ettringite precursor[19] were reported in our previous papers. In this work, the precursor of Zn–Al LDH also shows outstanding adsorption efficiency toward MO. Fig. 3 exhibits the adsorption kinetic experiment (left) and adsorption isotherm experiment (right) results of the precursor and Zn–Al LDH toward MO. The Zn–Al LDH displays a lower removal rate (43.69%) than that of the precursor (96.25%) toward MO after 120 min stirring. The adsorption isotherm experiment results show that the adsorption capacity of the precursor could reach about 250 mg g^{-1}, which is nearly the double that of the Zn–Al LDH (132 mg g^{-1}) toward MO. The Langmuir isotherm, which is assumed to undergo monolayer type coverage of the sorbent on an adsorbent surface,[21] was used to describe the obtained data of adsorption isotherm experiments as shown by the red line in Fig. 3. Eqn (1) represents the Langmuir isotherm model.
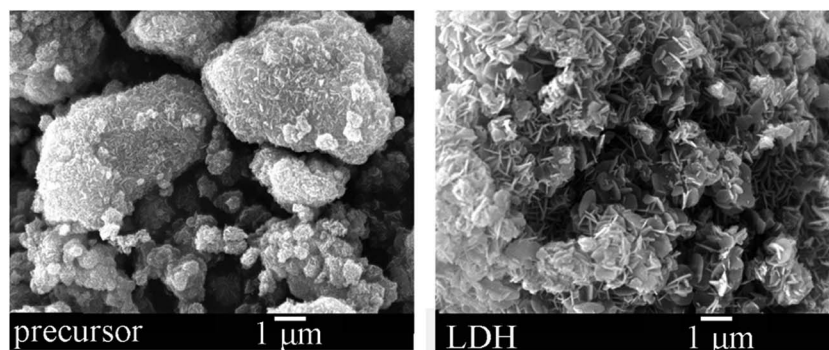
$$Q_e = Q_m \frac{bC_e}{1 + bC_e} \tag{1}$$

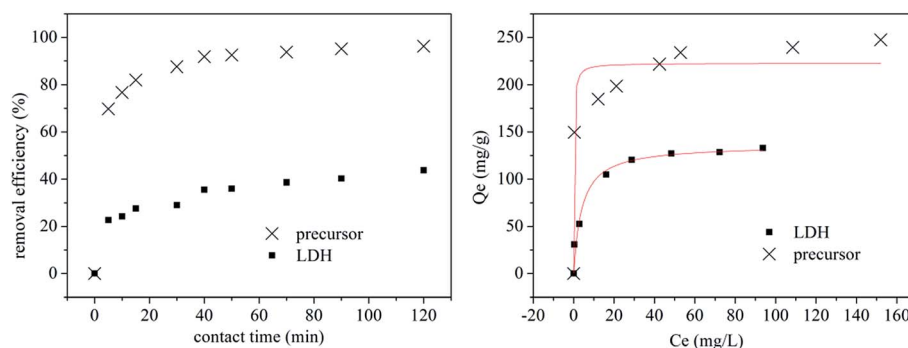**Fig. 2** SEM images of the precursor and LDH.

Fig. 3 Adsorption kinetic experiment (left) and adsorption isotherm experiment (right) results of the precursor and Zn–Al LDH toward MO. (C_e for equilibrium concentration, Q_e for adsorption capacity and red line for the Langmuir equilibrium isotherm.)

where, Q_e stands for the equilibrium adsorption capacity of MO adsorbed, C_e is the MO concentration at equilibrium and Q_m (mg g^{-1}) represents the theoretical maximum sorption capacity. The data of LDH fitted well with the Langmuir model (R^2 0.97), which suggests monolayer adsorption.[22] However, the data points of the precursor did not match well with the Langmuir isotherm model. Thus, it was supposed that another removal mechanism besides surface adsorption contributes to the enhanced adsorption performance of the precursor toward MO.

The adsorption kinetic experiment data were processed as pseudo-first order and pseudo-second order and the results are presented in Table 1. The rate constant of the precursor was higher than that of the LDH which indicates a higher adsorption rate for the removal of MO by the precursor. Furthermore, the pseudo-second order model was found to fit better with the correlation coefficient R^2 of 0.9961 and 0.9441 for the precursor and LDH, respectively, which are higher than that of the pseudo-first order model. The adsorption rate-determining steps for MO removal by the precursor and LDH were believed to be chemical absorption.

Zn–Al has been demonstrated to be an excellent photocatalyst for the degradation of organic pollutants.[7,23] In this work, more attention is paid not only to the adsorption property but also the photocatalytic performance of the precursor toward MO.

The contact area between a photocatalyst and organic pollutants is believed to have a massive impact on its photocatalytic efficiency. A higher contact area often results in a better photocatalytic performance.[3,20] The adsorption experiments demonstrate that the precursor could adsorb more MO molecules into its structure, or in other words, the precursor provides a higher contact area for the MO molecules which might promote the photocatalytic decoloration efficiency. To confirm this assumption, the photocatalytic performance of the precursor and LDH for the decoloration of MO solution was determined and the results are displayed in Fig. 5.

Fig. 4 exhibits the experimental data of the photocatalytic decoloration of MO (initial concentration 100 ppm) in aqueous solution by the precursor and as-prepared Zn–Al LDH and the comparison in the remaining MO concentrations by the precursor (A1 with irradiation and A2 without irradiation) and the LDH (B1 with irradiation and B2 without irradiation). The precursor could remove MO up to almost 100% under irradiation, whereas the LDH sample reached a removal rate of only 63% under the same conditions. A better adsorption performance of the precursor toward MO without light irradiation was also observed with an 84% removal rate for the precursor and 56% for the LDH, where a similar improvement in adsorption capacity by the precursor to that of the synthesized LDH was reported for the Mg–Al LDH sample.[18]

Although a further decrease in the remaining MO concentrations after the treatment of light irradiation to the adsorption operation was observed on both the precursor and LDH samples, a larger decrease by 15.23 mg L^{-1} was observed with the precursor than that of the LDH sample by 7.10 mg L^{-1}, which indicates higher photocatalytic activity by the precursor sample. It is understood that it is more difficult for the photocatalyst to degrade pollutants at low concentrations. The precursor realized enhanced photocatalytic performance in a relatively low concentration of MO which also proves the improvement in photochemical catalytic ability. For a clear description of the photocatalytic decoloration results, a pseudo-first order model was used to fit the kinetic curve of the MO photocatalytic decoloration, as shown in Table 2. High correlation coefficient R^2 values were obtained, which indicates that the pseudo-first-order model well explains the kinetic curve of MO photocatalytic decoloration. The highest rate constant was observed for the photocatalytic decoloration of MO by the precursor, which indicates the highest reaction rate. The

Table 1 Rate constant and correlation coefficient of the pseudo-first order $q_t = q_e(1 - e^{-k_1 t})$ and pseudo-second order $q_t = k_2 q_e^2 x/(1 + k_2 q_e t)$ for MO adsorption[a]

Model	Pseudo-first order			Pseudo-second order		
Parameters	k_1	R^2	q_e (mg g^{-1})	k_2	R^2	q_e (mg g^{-1})
Precursor	0.2406	0.9729	114.3019	0.0038	0.9961	120.4404
LDH	0.1102	0.8779	46.9974	0.0029	0.9441	52.4855

[a] Where, k_1 and k_2 are the rate constants, q_t is the amount of solute adsorbed on the adsorbent at time t, and q_e is the amount at equilibrium.
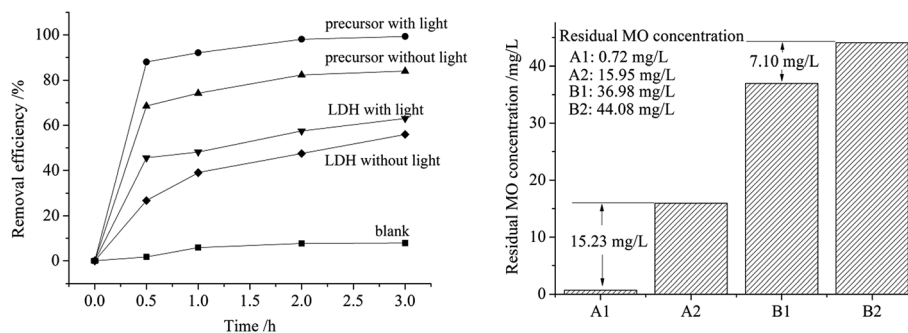

Fig. 4 Photocatalytic decoloration efficiency of MO by the precursor and Zn–Al LDH (left) and the difference in the remaining MO concentrations by the precursor (A1 with irradiation and A2 without irradiation) and LDH (B1 with irradiation and B2 without irradiation) (right).

Table 2 Rate constant (k), correlation coefficient (R^2) and disposal capability (q_e) of the pseudo-first order model for MO photocatalytic decoloration[a]

Parameter	Pseudo-first order $q_t = q_e(1 - e^{-kt})$		
	k	R^2	q_e
Precursor with light	4.5620	0.9959	121.3376
Precursor without light	3.4225	0.9914	102.0477
LDH with light	2.5042	0.9647	73.7035
LDH without light	1.2396	0.9893	68.8201

[a] Where, k_1 is the rate constant, q_t is the amount of solute adsorbed on the adsorbent at time t, and q_e is the amount at equilibrium.

simulated q_e was 121.33 mg L^{-1} and 102.05 mg L^{-1} with a gap of 18.83 mg L^{-1} for the precursor with or without irradiation, respectively, whereas the gap for LDH with or without light was 4.88 mg L^{-1} which is much less than that of the precursor. Both the experimental and simulated data prove the enhanced photocatalytic performance of the precursor for the photocatalytic decoloration of MO. We believe that the improvement in photocatalytic activity might result from the physically closer contact of the MO to the adsorbent, as confirmed by the higher removal efficiency in the adsorption section. This simply prepared precursor in a state of massive agglomeration demonstrates better adsorption for MO molecules when dispersed in MO solution, and decomposes the adsorbed MO compositions much more easily when irradiated under ultraviolet light. Thus, the precursor sample exhibits good performances for both adsorption and catalysis.

3.2 Discussion

3.2.1 The mechanism of enhanced adsorption. The enhanced adsorption performance of the Mg–Al–OH LDH precursor toward MO was reported in our previous paper,[18] in which no MO intercalation reaction was observed because the OH$^-$ anion of the precursor of Mg–Al–OH LDH could not exchange with the MO molecule. Thus, it could be concluded that the enhanced adsorption performance of the Mg–Al–OH

LDH precursor toward MO is a result of the disorderly state of the precursor, which could provide more adsorption sites than the closed structure of the LDH. In this work, the precursor of Zn–Al–CO$_3$ not only offered more adsorption sites but also directly reacted with MO molecules to produce MO intercalated LDH for the removal of MO molecules.[24,25]

Fig. 5 shows the XRD patterns of LDH, L-MO-LDH (LDH sample with MO adsorption) and P-MO-LDH (the precursor sample with MO adsorption). New peaks at $d_{003} = 2.5$ nm and $d_{006} = 1.24$ nm were observed in both L-MO-LDH and P-MO-LDH which could be attributed to the phase of MO intercalated LDH.[26] The peak intensity represents the content of the corresponding material. To compare the relative amount of MO intercalated LDH in the L-MO-LDH and P-MO-LDH samples, eqn (2) was applied.

$$R = \frac{I_m}{I_l} \qquad (2)$$

where, R represents the coefficient of relative amount of MO intercalated LDH, I_m and I_l are the diffraction intensity (d_{003} diffraction peak) of MO intercalated LDH and Zn–Al LDH in L-MO-LDH and P-MO-LDH, respectively. A higher R value indicates a higher content of MO intercalated LDH in the corresponding sample. The R value of P-MO-LDH was 1.51 which is a much higher than that of L-MO-LDH (0.28). This indicates that more MO molecules could be intercalated in the gallery space of the LDH forming MO intercalated Zn–Al LDH by the precursor which is illustrated by the adsorption model shown in Fig. 5. The higher efficiency of intercalation reaction contributed to the higher adsorption removal rate of the precursor toward MO than that of the Zn–Al LDH.

Besides the XRD characterization with the typical appearances of MO intercalated LDH, IR analysis is another effective way to describe the MO intercalation reaction of Zn–Al LDH. Fig. 6 displays the FT-IR spectra of LDH, P-MO-LDH, L-MO-LDH and MO. The LDH sample shows the typical FT-IR spectrum of Zn–Al–CO$_3$ LDH,[27] in which the broad absorption band at 3461 cm^{-1} is due to the O–H stretching of the hydroxyl groups. The peaks below 1000 cm^{-1} are attributed to the lattice vibration bands of M–O (M = Zn and Al). The peaks at 1364 cm^{-1}, 1492
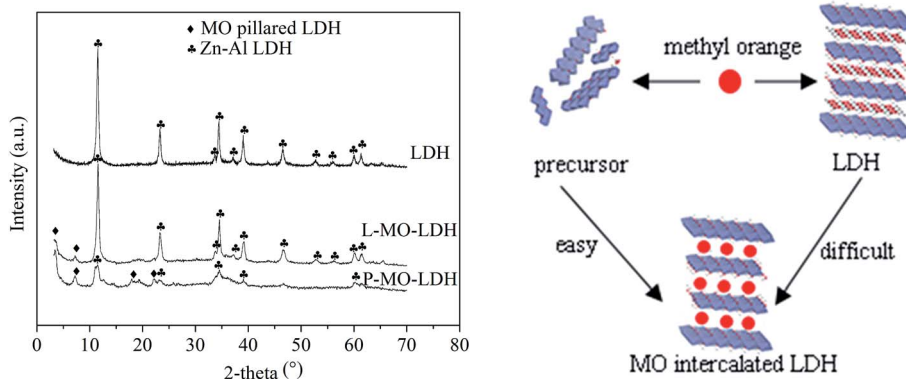

Fig. 5 XRD patterns (left) of LDH, L-MO-LDH (LDH sample with MO adsorption) and P-MO-LDH (the precursor sample with MO adsorption) and the adsorption model (right) of the precursor and LDH.
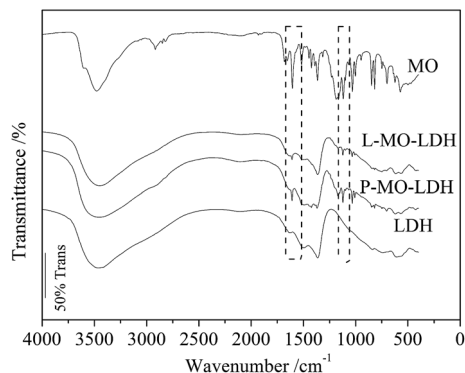
Fig. 6 FT-IR patterns of LDH, P-MO-LDH, L-MO-LDH and MO.

cm^{-1} and $1620\ cm^{-1}$ result from the asymmetric stretching vibrations of the interlayer carbonate anions, the ν_3 vibrations of the carbonate and the infrared bands of free water, respectively. After MO adsorption, the typical infrared bands of the MO molecule such as $1606\ cm^{-1}$ (N=N stretching) and $1119\ cm^{-1}$ (the vibrations of $-SO_3$) are clearly observed in the spectra of P-MO-LDH ($1609\ cm^{-1}$ and $1122\ cm^{-1}$, respectively) and L-MO-LDH ($1609\ cm^{-1}$ and $1123\ cm^{-1}$, respectively) as shown by the dashed box in Fig. 7. The transmittance of the bands is a reflection of the corresponding material content in the sample. It is observed that the transmittance of the peaks at around $1609\ cm^{-1}$ (N=N stretching) and $1122\ cm^{-1}$ (the vibrations of $-SO_3$) is lower for P-MO-LDH than that of L-MO-LDH, which indicates more MO molecules exist in P-MO-LDH and is consistent with the results in Fig. 5.

From the results in Fig. 5 and 6, it can be concluded that two mechanisms contributed to the enhanced adsorption activity of the precursor: the disorderly precursor could provide more adsorption sites than the closed structure of Zn–Al LDH for MO removal and the precursor could intercalate more MO molecules into the gallery space of LDH than that of the Zn–Al LDH.

3.2.2 The mechanism of enhanced photocatalytic activity.
Fig. 7 shows the UV-vis adsorption spectra and plots of $(Ah\nu)^2$ vs. $h\nu$ of the raw materials mixture, the precursor and the LDH sample. The raw materials displayed absolutely no photo absorption properties. The precursor prepared by dry milling of raw materials exhibited an obvious light absorption edge in the

ultraviolet region and the adsorption edge of the Zn–Al LDH became more sensitive. The energy gaps of the prepared samples were calculated according to the following equation described in a previous work.[28]

$$Ah\nu = K(h\nu - E_g)^{n/2} \quad (3)$$

where, A, h, ν, K and E_g represent the absorption coefficient, Planck constant, light frequency, proportionality constant, and band gap, respectively. Here, $n = 1$ for LDH.[28] Fig. 7 displays the plot of $(Ah\nu)^2$ vs. $h\nu$ for the determination of band gaps, which gives values of 3.35, 3.26 and 5.53 eV for the precursor, LDH sample and raw materials mixture, respectively. These values are in accord with other reported band gaps of Zn–Al LDH (3.0–3.2 eV).[29]

We reported that the co-grinding of raw materials to produce an amorphous precursor is essential for its adsorption properties in our previously published work on the precursor of Ca–Al for Cr(VI) removal.[30] The co-existence of the raw materials or simply mixed separately milled materials showed no obvious adsorption behavior for anionic pollutants. Combining the results of the UV-vis adsorption spectra and band gaps of the prepared samples, it can be concluded that dry milling induced a chemical reaction between the raw materials, forming the basic structure of Zn–Al LDH which enhanced the photocatalytic action for MO molecules.

Close contact between the photocatalyst and the organic pollutant is essential for the photocatalytic reaction. Increasing the specific surface area of the photocatalyst or dispersing the photocatalyst in porous supporting materials provides a higher contact area for the photocatalyst to decompose organic pollutants.[20] In this precursor system, the enhanced photocatalytic activity of the precursor also from the high contact area of the photocatalyst. It has been proven that the precursor could provide more adsorption sites for MO molecules and intercalate more MO molecules into its gallery space. In other words, the contact area between the precursor and MO molecules was definitely higher than that of the LDH.

Fig. 8 displays the XRD patterns of the precursor and LDH samples dispersed in MO solution with or without irradiation. Without light irradiation, in the patterns of both samples, besides the peaks of Zn–Al LDH phases, new peaks at $d_{003} = 2.5$ nm and $d_{006} = 1.24$ nm are observed which could be
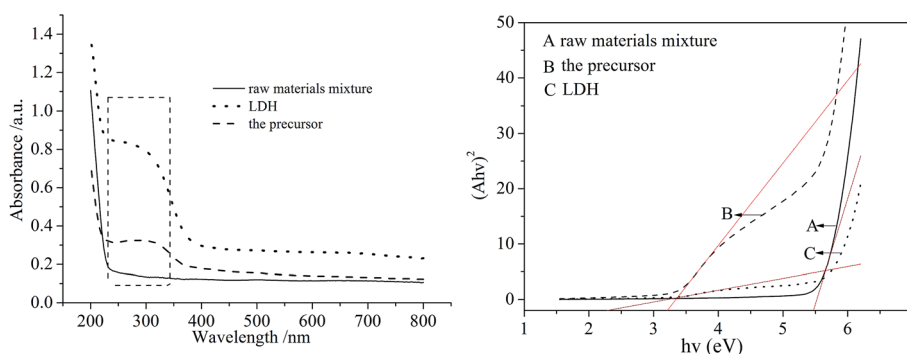

Fig. 7 UV-vis adsorption spectra (left) and plots of $(Ah\nu)^2$ vs. $h\nu$ (right) for the raw materials mixture, precursor and LDH samples.
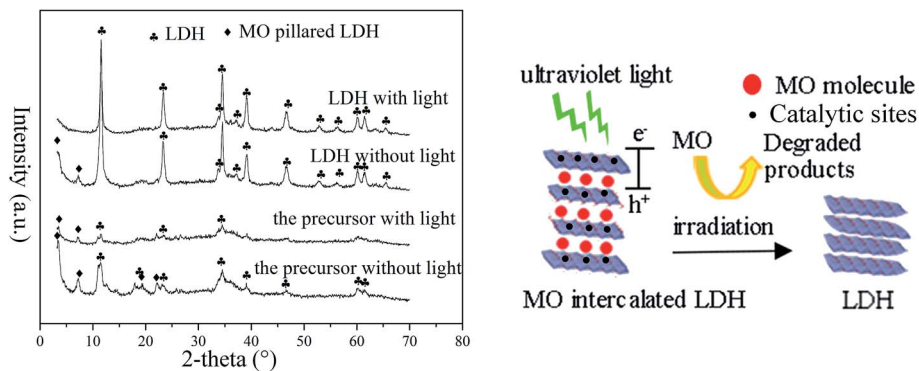
Fig. 8 XRD patterns (left) of the used samples for the removal of MO with or without irradiation and the photocatalytic model (right) of the precursor and LDH.

attributed to the phase of MO intercalated LDH.[23] The peak intensity of MO intercalated LDH from the precursor sample is much higher than that from the LDH sample, which confirms the higher adsorption of MO. With light irradiation, the peaks of MO intercalated LDH from the LDH sample disappeared completely and became much lower for the precursor sample. As is well known, the photocatalytic reaction degrades organic molecules on the surface of photocatalysts such as TiO_2.[31] In the case of LDH, the photocatalytic activity sites came from the layered sheets of the LDH. The catalytic sites in the internal space might not work well if the organic pollutant is just adsorbed on the surface, which is quite a long distance from the activity sites. MO intercalation makes it possible for the efficient use of catalytic sites in the internal space as well as that on the surface. In other words, the contact area between the photocatalyst and organic pollutants could be increased when a intercalation reaction takes place. The results in Fig. 8 demonstrate that the photocatalytic properties of LDH came from the sheets of the Zn–Al LDH and intercalated MO molecules were decomposed in the gallery space, as the photocatalytic model shows in Fig. 8. The precursor could intercalate more MO molecules into the layered space of LDH to contact with the sheets of the LDH, which means a higher contact area between MO and the precursor, resulting in the higher photocatalytic efficiency of the precursor.

Many previous works have established and discussed the photocatalytic activities of Zn type LDH.[32,33] Zn–Al LDH could produce two main intermediate active species (superoxide $O_2^{\cdot-}$ and hydroxyl radicals $OH^{\cdot}$) under irradiation for the photocatalytic decoloration of MO. Clear evidence[29,33] has proven that $O_2^{\cdot-}$ plays the main role in the initiation of the photocatalytic process in LDH photocatalytic systems.

The LDH samples are well known anionic absorbents, which exhibit high capacity toward anionic organic samples such as MO in this work. On the other hand, very low adsorption capacity was observed with the cationic reagent RHB. To verify our assumption that the excellent adsorption performance of the precursor contributes to the enhanced photocatalytic activity, the photocatalytic decoloration of RHB (initial concentration 4 ppm) by the precursor and as-prepared Zn–Al

LDH, in which no adsorption process was involved, was conducted as a reference experiment, and the results are shown in Fig. 9. Without light irradiation, no obvious changes in the remaining RHB concentration were observed on both the precursor and Zn–Al LDH samples, which confirm that they have no adsorption ability toward RHB. Under irradiation, both samples exhibited photocatalytic activity toward RHB and higher efficiency was obtained by the LDH sample than the precursor. Without the adsorption action in this case, it was reasonable to obtain higher photocatalytic efficiency by using the Zn–Al LDH than the precursor sample due to the much better crystallinity, dispersion state and light adsorption of the Zn–Al LDH, as shown in Fig. 1, 2 and 4. These results from RHB reflect that in the case of the precursor to the MO, there exists a synergistic effect of both adsorption and photocatalytic action to enhance the removal efficiency, which is as high as close to complete decoloration.

The data from both MO and RHB confirm the photocatalytic action of the precursor and Zn–Al LDH samples prepared *via* a simple milling operation. The precursor sample shows enhanced adsorption and photocatalytic activity compared to that of the Zn–Al LDH sample toward MO. The disordered precursor provides more adsorption sites and intercalates more
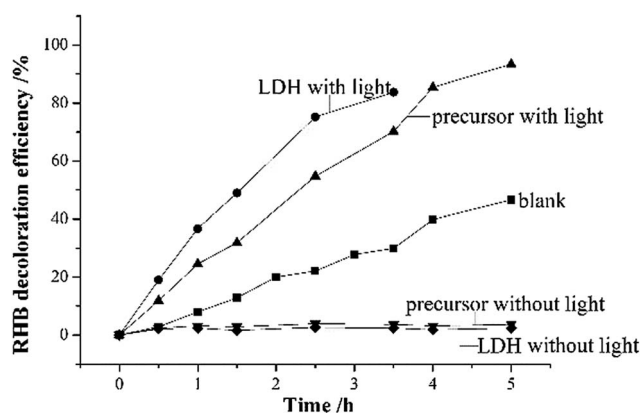

Fig. 9 Photocatalytic decoloration of RHB by the precursor and as-prepared Zn–Al LDH.

MO molecules into the gallery space of LDH than the closed structure of Zn–Al LDH for MO removal. Thus, a high contact area between the precursor and MO was obtained which resulted in enhanced adsorption and photocatalytic activity. The efficient MO removal almost to complete decoloration particularly on the precursor sample at a relatively high concentration confirms that this method could produce photocatalysts with a high performance at a low cost. Another obvious advantage is that hydroxides and carbonates, which are stable, cheap and easily available compared with the soluble nitrate or sulfate salts of zinc and aluminium used by the co-precipitation method, are directly used as starting samples to prepare the products without emission of other impurities and wastewater. We believe that the precursor prepared by this method could be applied as photocatalyst and would contribute to real wastewater treatment due its overall super performance as a result of the synergistic effect of its adsorption and catalysis capacity.

4 Conclusions

An amorphous precursor of the Zn–Al LDH photocatalyst was simply prepared by dry milling $Zn_4CO_3(OH)_6 \cdot H_2O$ and $Al(OH)_3$. The precursor intercalates more MO molecules into the layered space of LDH to contact with the sheets of the LDH and exhibits super a photocatalytic performance toward MO decoloration based on the synergistic effects of intercalation reaction and catalysis. This useful sample could be easily obtained without elaborate efforts to prepare fine particles with high specific surface areas or composites to disperse the catalyst in a supporting material to increase both adsorption and catalysis performances, thus offering a cheap alternative to contribute to wastewater treatment at a reasonably low cost. The idea of using the precursor instead of the synthesized final product may serve other purposes where the close access of the target sample by adsorption is required.

Acknowledgements

References

1 S. J. Xia, F. X. Liu, Z. M. Ni, J. L. Xue and P. P. Qian, Layered double hydroxides as efficient photocatalysts for visible-light degradation of rhodamine B, *J. Colloid Interface Sci.*, 2013, **405**, 195–200.

2 Z. Yang, F. Wang, C. Zhang, G. Zeng, X. Tan, Z. Yu, Y. Zhong, H. Wang and F. Cui, Utilization of LDH-based materials as potential adsorbents and photocatalysts for the decontamination of dyes wastewater: a review, *RSC Adv.*, 2016, **6**, 79415–79436.

3 K. M. Parida and L. Mohapatra, Carbonate intercalated Zn/Fe layered double hydroxide: a novel photocatalyst for the enhanced photo degradation of azo dyes, *Chem. Eng. J.*, 2012, **179**, 131–139.

4 J. S. Valente, F. Tzompantzi, J. Prince, J. G. H. Cortez and R. Gomez, Adsorption and photocatalytic degradation of phenol and 2,4-dichlorophenoxiacetic acid by Mg–Zn–Al layered double hydroxides, *Appl. Catal., B*, 2009, **90**, 330–338.

5 K. Dutta, S. Das and A. Pramanik, Concomitant synthesis of highly crystalline Zn–Al layered double hydroxide and ZnO: phase interconversion and enhanced photocatalytic activity, *J. Colloid Interface Sci.*, 2012, **366**, 28–36.

6 B. Lin, P. Sun, Y. Zhou, S. Jiang, B. Gao and Y. Chen, Interstratified nanohybrid assembled by alternating cationic layered double hydroxide nanosheets and anionic layered titanate nanosheets with superior photocatalytic activity, *J. Hazard. Mater.*, 2014, **280**, 156–163.

7 D. Carriazo, M. D. Arco, E. García-López, G. Marcì, C. Martín, L. Palmisano and V. Rives, Zn, Al hydrotalcites calcined at different temperatures: preparation, characterization and photocatalytic activity in gas–solid regime, *J. Mol. Catal. A: Chem.*, 2011, **342–343**, 83–90.

8 D. Basu, A. Das, D. Wang, J. J. George, K. W. Stöckelhuber, R. Boldt, A. Leuteritz and G. Heinrich, Fire-safe and environmentally friendly nanocomposites based on layered double hydroxides and ethylene propylene diene elastomer, *RSC Adv.*, 2016, **6**, 26425–26436.

9 Á. Deák, L. Janovák, E. Csapó, D. Ungor, I. Pálinkó, S. Puskás, T. Ördög, T. Ricza and I. Dékány, Layered double oxide (LDO) particle containing photoreactive hybrid layers with tunable superhydrophobic and photocatalytic properties, *Appl. Surf. Sci.*, 2016, **389**, 294–302.

10 W. Tongamp, Q. Zhang and F. Saito, Preparation of meixnerite (Mg–Al–OH) type layered double hydroxide by a mechanochemical route, *J. Mater. Sci.*, 2007, **42**, 9210–9215.

11 W. Tongamp, Q. Zhang and F. Saito, Mechanochemical route for synthesizing nitrate form of layered double hydroxide, *Powder Technol.*, 2008, **185**, 43–48.

12 J. Qu, Q. Zhang, X. He and S. Song, Mechanochemical approaches to synthesize layered double hydroxides: a review, *Appl. Clay Sci.*, 2016, **119**, 185–219.

13 J. Qu, X. He, B. Wang, L. Zhong, L. Wan, X. Li, S. Song and Q. Zhang, Synthesis of Li–Al layered double hydroxides via a mechanochemical route, *Appl. Clay Sci.*, 2016, **120**, 24–27.

14 J. Qu, L. Zhong, Z. Li, M. Chen, Q. Zhang and X. Liu, Effect of anion addition on the syntheses of Ca–Al layered double hydroxide via a two-step mechanochemical process, *Appl. Clay Sci.*, 2016, **124–125**, 267–327.

15 J. Qu, X. Li, Z. Lei, Z. Li, M. Chen and Q. Zhang, Mechano-hydrothermal synthesis of tetraborate pillared Li–Al layered double hydroxides, *J. Am. Ceram. Soc.*, 2016, **99**, 151–1154.

16 Z. Ferencz, M. Szabados, M. Ádok-Sipiczki, K. Ákos, Z. Kónya, P. Sipos and I. Pálinkó, , Mechanochemically assisted synthesis of pristine Ca(ɪɪ)Sn(ɪv)-layered double hydroxides and their amino acid intercalated nanocomposites, *J. Mater. Sci.*, 2014, **49**, 8478–8486.

17 Zs. Ferencz, M. Szabados, G. Varga, Z. Csendes, Á. Kukovecz, Z. Kónya, S. Carlson, P. Sipos and I. Pálinkó, Mechanochemical synthesis and intercalation of Ca(ɪɪ)

Fe(III)-layered double hydroxides, *J. Solid State Chem.*, 2016, **233**, 236–243.

18 B. Wang, J. Qu, X. Li, X. He and Q. Zhang, Precursor preparation to promote the adsorption of Mg–Al layered double hydroxide, *J. Am. Ceram. Soc.*, 2016, **99**, 2882–2885.

19 L. Zhong, J. Qu, X. Li, X. He and Q. Zhang, Simultaneous synthesis of ettringite and absorbate incorporation by aqueous agitation of a mechanochemically prepared precursor, *RSC Adv.*, 2016, **6**, 35203–35209.

20 Z. Sun, Z. Hu, Y. Yan and S. Zheng, Effect of preparation conditions on the characteristics and photocatalytic activity of TiO_2/purified diatomite composite photocatalysts, *Appl. Surf. Sci.*, 2014, **314**, 251–259.

21 L. Ma, Q. Wang, S. M. Islam, Y. Liu, S. Ma and M. G. Kanatzidis, Highly selective and efficient removal of heavy metals by layered double hydroxide intercalated with the MoS_4^{2-} ion, *J. Am. Chem. Soc.*, 2016, **138**, 2858–2866.

22 A. Farrukh, A. Akram, A. Ghaffar, S. Hanif, A. Hamid, H. Duran and B. Yameen, Design of polymer-brush-grafted magnetic nanoparticles for highly efficient water remediation, *ACS Appl. Mater. Interfaces*, 2013, **5**, 3784–3793.

23 E. M. Seftel, E. Popovici, M. Mertens, K. D. Witte, G. V. Tendeloo, P. Cool and E. F. Vansant, Zn-Al layered double hydroxides: synthesis, characterization and photocatalytic application, *Microporous Mesoporous Mater.*, 2008, **113**, 296–304.

24 L. Mohapatra, D. Patra, K. Parida and S. J. Zaidi, Enhanced Photocatalytic Activity of a Molybdate-Intercalated Iron-Based Layered Double Hydroxide, *Eur. J. Inorg. Chem.*, 2017, **3**, 723–733.

25 L. Mohapatra and K. Parida, A review on the recent progress, challenges and perspective of layered double hydroxides as promising photocatalysts, *J. Mater. Chem. A*, 2016, **4**, 10744–10766.

26 P. Zhang, G. Qian, H. Shi, X. Ruan, J. Yang and R. L. Frost, Mechanism of interaction of hydrocalumites (Ca/Al-LDH)

with methyl orange and acidic scarlet GR, *J. Colloid Interface Sci.*, 2012, **365**, 110–116.

27 K. Yang, L. G. Yan, Y. M. Yang, S. J. Yu, R. R. Shan, H. Q. Yu, B. C. Zhu and B. Du, Adsorptive removal of phosphate by Mg–Al and Zn–Al layered double hydroxides: kinetics, isotherms and mechanisms, *Sep. Purif. Technol.*, 2014, **124**, 36–42.

28 S.-J. Xia, F.-X. Liu, Z.-M. Ni, W. Shi, J.-L. Xue and P.-P. Qian, Ti-based layered double hydroxides: Efficient photocatalysts for azo dyes degradation under visible light, *Appl. Catal., B*, 2014, **144**, 570–579.

29 H. Li, Q. Deng, J. Liu, W. Hou, N. Du, R. Zhang and X. Tao, Synthesis, characterization and enhanced visible light photocatalytic activity of Bi_2MoO_6/Zn–Al layered double hydroxide hierarchical heterostructures, *Catal. Sci. Technol.*, 2014, **4**, 1028–1037.

30 L. Zhong, X. He, J. Qu, X. Li, Z. Lei, Q. Zhang and X. Liu, Precursor preparation for Ca-Al layered double hydroxide to remove hexavalent chromium coexisting with calcium and magnesium chloride, *J. Solid State Chem.*, 2017, **245**, 200–206.

31 D. P. Kumar, N. L. Reddy, M. Karthikeyan, N. Chinnaiah, V. Bramhaiah, V. D. Kumari and M. V. Shankar, Synergistic effect of nanocavities in anatase TiO_2, nanobelts for photocatalytic degradation of methyl orange dye in aqueous solution, *J. Colloid Interface Sci.*, 2016, **477**, 201–208.

32 K. Parida, L. Mohapatra and N. Baliarsingh, Effect of Co^{2+} substitution in the framework of carbonate intercalated Cu/Cr LDH on structural, electronic, optical, and photocatalytic properties, *J. Phys. Chem. C*, 2012, **116**, 22417–22424.

33 L. Mohapatra, K. Parida and M. Satpathy, Molybdate/tungstate intercalated oxo-bridged Zn/Y LDH for solar light induced photodegradation of organic pollutants, *J. Phys. Chem. C*, 2012, **116**, 13063–13070.